Advances in Materials Technology for Fossil Power Plants
Proceedings from the Eighth International Conference
October 11–14, 2016, Albufeira, Algarve, Portugal
https://doi.org/10.31399/asm.cp.am-epri-2016p0260

J. Parker, J. Shingledecker, J. Siefert, editors

DESIGN, OPERATION, NUMERICAL SIMULATION AND DAMAGE ASSESSMENT OF A HEADER IN THE HWT TEST LOOP

Magdalena Speicher, Andreas Klenk
Material Testing Institute University of Stuttgart, Stuttgart, Germany
Tobias Steck, Andreas Helmrich, Frank Kluger
GE Boiler, Stuttgart, Germany

ABSTRACT

In the test loop HWT II (High Temperature Materials Test Loop) installed in the fossil power plant Grosskraftwerk (GKM) Mannheim in Germany, thick-walled components made of nickel base alloys were operated up to temperature of 725 °C. The operation mode chosen (creep-fatigue) was to simulate a large number of start-ups and shutdowns with high gradients as expected for future high efficient and flexible power plants and to investigate the damage due to thermal fatigue of the used nickel base alloys.
In this paper the damage evolution of a header made of the nickel base alloys Alloy 617 B and Alloy C263, which was a part of HWT II test rig, were investigated using nondestructive and destructive techniques.
Furthermore, the damage has been considered and evaluated by using numerical methods. In addition, different lifetime assessment methods of standards and recommendations with focus on creep-fatigue damage were used and evaluated. The different lifetime models are applied to the header and the results were compared to the results of metallographic investigations and damage observations.

INTRODUCTION

In Grosskraftwerk Mannheim a material test loop was installed, in which thick-walled components for future high-efficient power plants were operated stationary and non-stationary at steam temperatures up to 725 °C. Within the project a basic knowledge of the material behavior was determined, which allows an assessment of key components such as headers, pipes, pipe bends and valves made of nickel alloys. The test loop was installed in Unit 6 in GKM and was operated from October 2012 to April 2014. The flow chart of the test rig is shown in Fig. 1.
The main aims of the investigation of the components in the test loop included:

- Relaxation behavior of components at superimposed secondary stresses,
- Fatigue and damage behavior by thermally induced stresses during thermal cycling within the temperature range from 400 °C to 725 °C,
- Functionality of the high-temperature control valves.

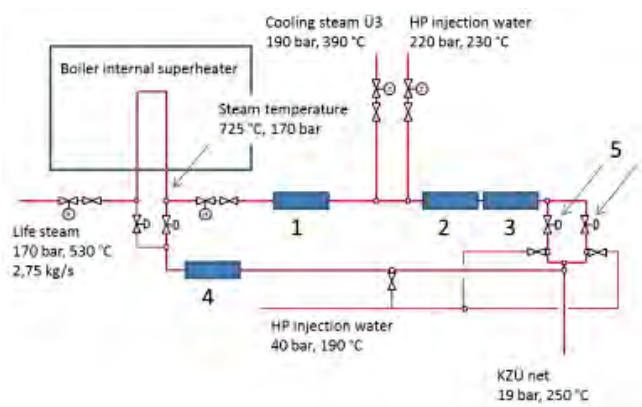

Figure 1: Flow chart of test rig HWT II

By injecting cooling water and steam in the temperature range between 400 °C and 725 °C 14 thermal load cycles per day were realized. Thus, an operating time of 9,900 hours at temperatures of over 700 °C and 2,638 thermal cycles could be reached during the duration of the research project.
One of the key components in the test section was a header, which was operated in the non-stationary part of the test loop. In the next sections the operation and the damage behavior of the header will be considered in more detail.

MANUFACTURING AND OPERATION OF THE HEADER

Fig. 2 shows the drawing of the header and its installation in the test loop. A thick-walled pipe (body) was the basis of the header subjected to the main steam. The component had five bypasses (thin-walled boiler tubes that have been welded with their respective entry and exit openings perpendicularly to the thick-walled pipe. In order to get a mass flow in the bypass tubes the cross-section of the main pipe was reduced. The entry of the pipe was made of the Alloy 617 B and the exit was made of Alloy C263. Thick-walled pipes of dimension ø 220 mm x 50 mm were forged, hollow drilled and welded together (TIG orbital). The seam between the two pipes was welded with filler material Alloy 617 B. The bypass tubes were connected with the thick-walled pipe via a short header nipple. For this similar materials were chosen. Thinwalled straight tubes and bends build the bypass. Tubes and Bends were manufactured on the inlet side of Alloy 617 B and the outlet side of Alloy 740.

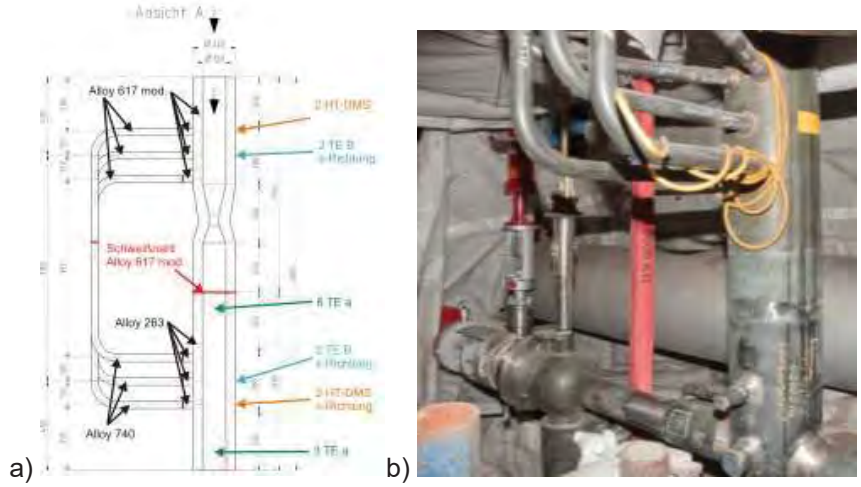

Figure 2: a) Technical drawing of the header, b) Installation of the header in the test loop

The chemical composition and the heat treatment of the materials Alloy 617B and Alloy C263 are summarized in Tab. 1. The chemical composition corresponds to the respective specifications of the alloys [1, 2]. After welding, the component was subjected to a heat treatment (PWHT) at 980 °C for 3 hours, followed by precipitation hardening at 800 °C for 4 h.

Table 1: Chemical composition and heat-treatment conditions of materials investigated

	Chemical composition (wt.%)							
Material	C	Cr	Mo	Co	Al	Ti	Fe	Other
Alloy 617B	0,064	22,3	8,72	11,3	1,17	0,46	0,46	B:0,0034
Alloy 263	0,060	19,8	5,8	19,9	0,50	2,10	0,40	B: 0,0020
	Parameters of heat treatment							
Alloy 617B	1200 °C / 3 h / Water + 980 °C / 3 h / Air							
Alloy 263	1150 °C / 2 h / Water + 800 °C / 4 h / Air							

To achieve a significant damage state in the header during the operation of the test loop, more than 2000 cycles were realized to simulate startup and shutdown events. To ensure that during the operational phase of the test loop damage could be observed in the component, various load scenarios were examined with different temperature gradients by numerical simulations before starting the test loop. These studies resulted in a temperature cycle lasting less than two hours (6,300 seconds). Based on these numerical pre-studies the control parameters of the steam and water injection into the test loop were chosen and programmed. In Fig. 3 the courses of measured steam temperature, internal pressure and mass flow during five cycles are shown as an example.

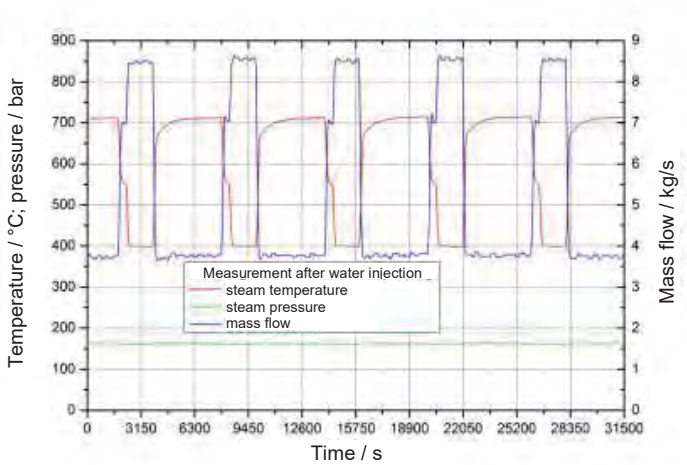

Figure 3: Measuring gradients of temperature, the internal pressure and the mass flow for five cycles

In the drawing, Fig. 2a the positions of the applied temperature and strain measurement points are marked. Four capacitive high temperature strain gauges (two in axial and two in hoop direction of the pipe) and 12 thermocouples were installed. Thus, a sufficient monitoring of the header during operation was guaranteed and this enabled a proper analysis of the recorded data for determining input data and for comparisons with numerical simulations.

DAMAGE CHARACTERISATION

Nondestructive testing

To perform non-destructive tests on the critical hole edge regions, the header was removed from the test loop after operation. In the first step all of the ten bore holes were observed using an endoscope. At all hole edges cracks were identified. To visualize the shape and depth of the cracks dye-penetrant tests were performed. The results of these testing are shown in Fig. 4.

Especially in the part made of Alloy 617 B clear crack indications are visible. Particularly in the third row in front of the laval nozzle distinctive cracks in the area of both edges of the holes were identified (Fig.4, left). In the area of Alloy C263 clear indications could be found in the fourth row, which was to be expected, since the left edge of the hole was carried out with a radius of 3 mm. The hole edges with radius 3 mm were subjected to detailed metallographic investigations (see green dotted-line in Fig. 4). The results of these examinations are shown in the next section.

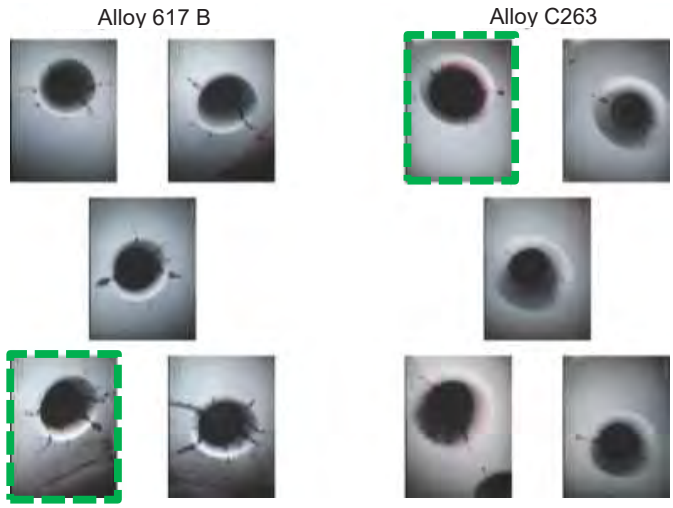

Figure 4: Results of dye-penetration testing of the hole edges of the header

Metallographic investigations

At the two selected hole edges in the area of Alloy 617 B and Alloy C263 metallographic sections were prepared and the cracks with the largest indications were broken (Fig. 5). The metallographic sections were thereby made parallel to the internal surface of the header and prepared according to state of the art. For the light-optical analyzes a light microscope was used.

The investigation of the two material areas showed that the cracks initiate transgranular at the edges of the holes on the inner surface, propagate also mainly transgranular into the base material (Fig. 6 and 7). The multiple cracks found are characteristic for (thermal)-fatigue damage. The intergranular contribution to crack growth was very low in both material regions. In the area of Alloy 617 B very low amount of creep cavities at the grain boundaries could be seen around the larger cracks. The density of the cavities decreased from the outside to the inside. For Alloy C263 no creep cavities were identified. Many cracks changed the propagation direction and only a low portion of grain boundaries was damaged. Some of the cracks in two material regions showed branches, mainly towards the crack tip. The deepest crack at the hole edge in the area of Alloy 617 B had a length of 9.1 mm and was significantly larger (Fig. 6, right) as the crack in Alloy C263 which was about 3.2 mm (Fig. 7, right).

The flanks of all cracks were filled with oxides and oxidation was observed at the near-surface region of Alloy 617B. The oxide layer of Alloy C263 was compact and only a slight difference in concentration at the grain boundaries close to the surface was determined.

From the examination of the fracture surface, similar damage features could be observed with regard to size of the cracks. The extension of the cracks and the crack configuration were comparable in both cases. It was found that in both materials the cracks were longer in the direction of the boiler tubes than the thick-walled pipe section.

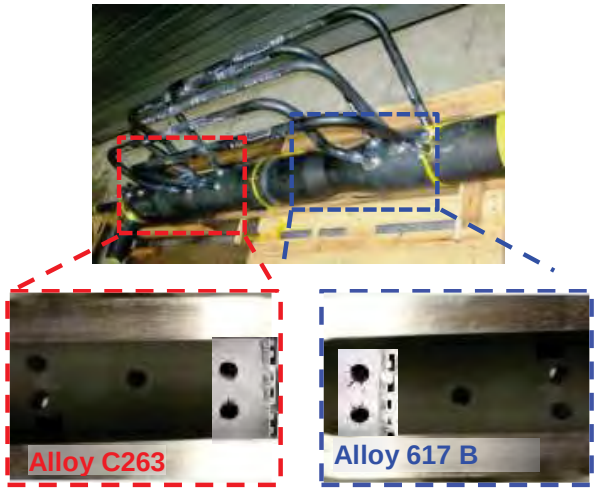

Figure 5: Cutting of the header after operation

The shape of the cracks resembled a quarter ellipse, which is an indicator for the fatigue crack propagation. The fracture surfaces were mostly uneven.
Following hardness HV 10 was measured in the area of the ligament in the two material areas: Alloy 617 B with 270 HV 10 and Alloy C263 with 297 HV10. Thus, a significant hardening during service occur for Alloy 617 B (initial state: 200 HV 10) and only a slight increase in the hardness of Alloy C263 (initial state: 265 HV 10) could be determined.

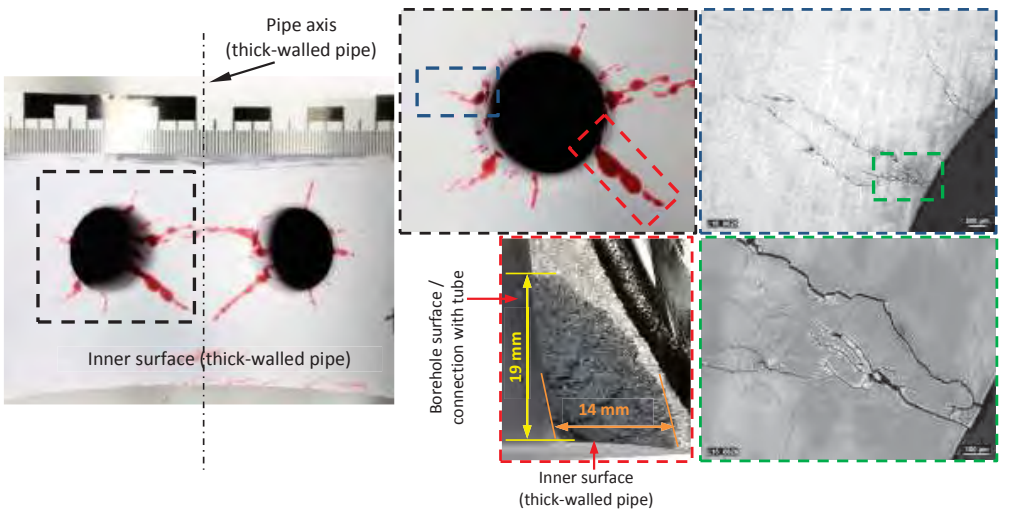

Figure 6: Investigations at the bore hole with 3 mm radius, material Alloy 617 B

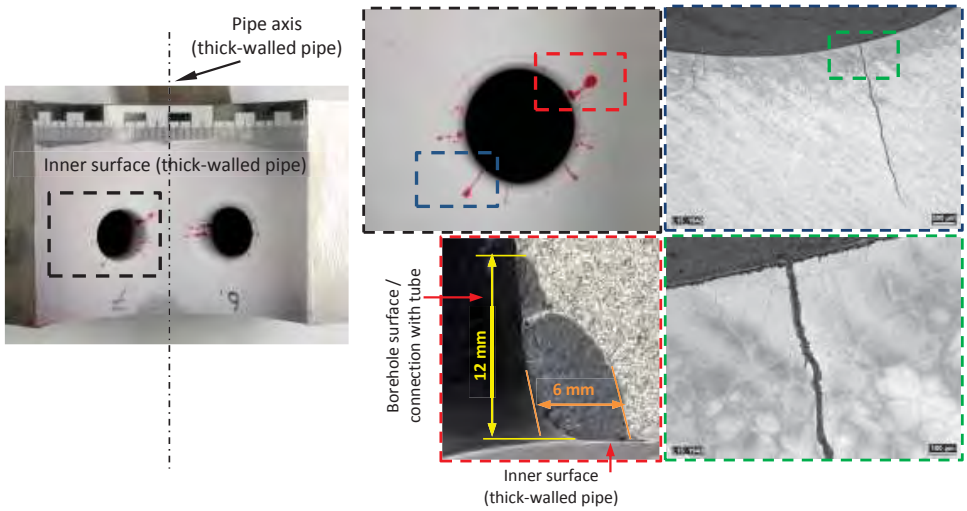

Figure 7: Investigations at the bore hole with 3 mm radius, material: Alloy C263

Numerical Investigations

A damage assessment of the header was performed using numerical methods, [14]. For this purpose, first the operation of the component was simulated. To describe the visco-plastic material behavior the CNOW model was used, details of the model are given in [3, 4, 5]. In the simulations the measured steam temperature profile, as well as the time courses of the heat transfer coefficients determined from the internal pressure, the mass flow and the steam temperature according to the formulas of the VDI Heat Atlas [6] (Fig. 3) m were considered. Five cycles were simulated. The internal pressure remained constant throughout the test loop operation with 170 bar. Figure 8 shows the fine Finite Element mesh and the mechanical boundary conditions used in the simulation of the header.

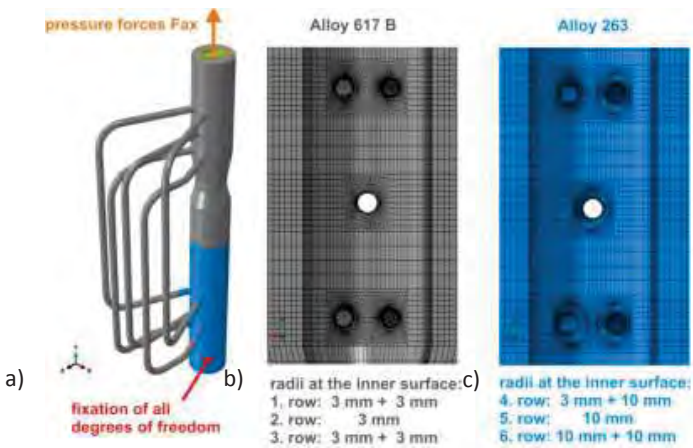

Figure 8: Boundary conditions of the performed simulation; a) the header, b) part made of Alloy 617 B, c) part made of Alloy C263

The development of stress, strain and temperature evaluated on the highly stressed position of the hole edge in the area of Alloy 617 B (Row 3 left, r = 3mm, see Fig. 8) are shown in Fig. 9 a and at the hole edge in the area of Alloy C263 (Row 4 left, r = 3mm, see Fig. 8) in Fig. 9 b. As a consequence of the two-stage cooling with steam and water two tensile stress and tensile strain maximum on the hole edges occur, whereas a compressive stress or strain maximum occur during the heating phase. Furthermore, it is evident that the

stresses resulting from the thermal cycles are almost symmetrical indicating cyclic loading without mean stress and cyclic plastic deformation. The greatest strain amplitudes over one cycle occur with about 0.42 % at the edge of the hole with 3 mm in the area of Alloy C263. In the area of the hole edge with a radius of 3 mm of Alloy 617 B the maximum strain amplitude is about 0.37 %. Looking at the extreme values of the stresses it could be shown that in Alloy C263 the level of tensile and compressive stresses is substantially higher than in Alloy 617 B. The hold time stresses present in both materials at the hole edges, amount in average to about 250 MPa.

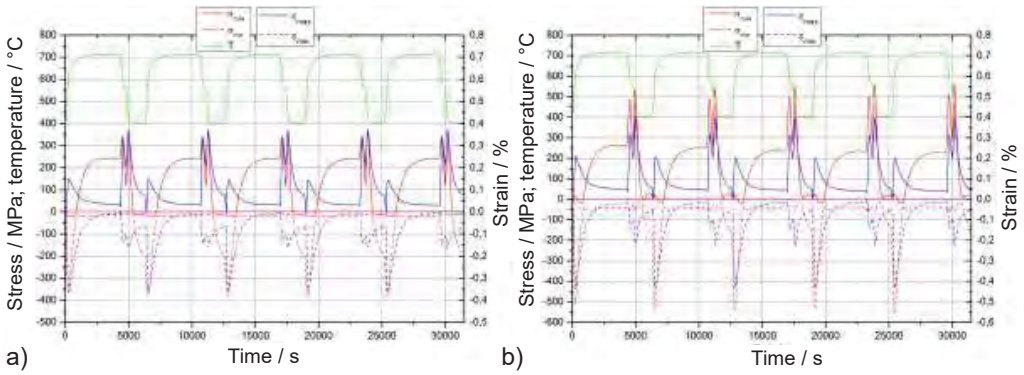

Figure 9: a) evaluation of the hole edge in the area of Alloy 617 B, row 3 left, r = 3mm, see Fig. 8; b) evaluation of the hole edge in the area of Alloy C263, row 4 left, r = 3mm, see Fig. 8

On the basis of the determined stresses different approaches were applied to assess the damage as well as the lifetime of the header. For this, various standards such as DIN EN-12952-3 / 4 [7, 8], ASME NH T-1400 [9], RCC-MR RB 3262.12 [10] or recommendations as R5 Volume 2/3 [11] can be used. The European DIN EN 12952-3/4 uses an elastic approach for the lifetime assessment, whereas in the American ASME Code Case, the French RCC-MR and the British R5 elastic and inelastic approaches are given. As shown by Eq.1 the determination of the total damage D in all approaches is carried out with the linear addition of the fatigue damage D_f and the creep damage D_c (Eq. 1):

$$D = D_f + D_C \tag{1}$$

In ASME and RCC-MR the total damage is assessed with material dependent damage envelopes. The material dependent damage envelope of Alloy 617 is taken from [12]. R5 recommendations and DIN EN 12952 use a material independent damage envelope, where in a purely linear accumulation the damage criteria is reached when the total damage exceeds a value of one.

For the calculation of the fatigue damage the knowledge of the allowable number of cycles N_A is necessary. The determination of the allowable number of cycles in terms of fatigue damage in ASME and RCC-MR is carried out with the equivalent strain range. In comparison R5 uses a fracture mechanics approach, the process is divided into a crack initiation and crack propagation phase until a defined critical (small) crack length is reached. The approach of the European standard DIN EN-12952 needs the temporal stress tensors of an elastic calculation for the determination of the relevant stress range, which is necessary to calculate the allowable number of cycles. In the approaches of all standards the fatigue damage is calculated by the Miner-Rule.

Determination of creep damage is carried out with the time fraction rule in DIN EN-12952, ASME and RCC-MR. The knowledge of stress σ and temperature T dependent rupture time t_r for dwell time t_{dwell} is necessary for the calculation of creep damage.

In DIN EN-12952-3/4 the relevant stress for the determination of the rupture time is calculated with the design equation under usage of the operating pressure. Then the lower scatter band of the creep rupture curve at maximum dwell temperature is used to identify the rupture time. The stress controlling creep damage is

determined with material dependent values, the principle stresses and the equivalent von Mises stress in ASME and RCC-MR.

The lifetime of components under creep-fatigue loading can also be obtained using phenomenological CDM-approaches. In this work the approach by Lemaitre [13] was chosen. The total damage is divided into a fatigue damage part, which mainly depends on the plastic strain range Δp and a creep damage portion, which mainly depends on the equivalent Mises stress. The Heaviside function H in the creep damage equation is added to the original formulation of Lemaitre and acts as a switch. When the maximum principle strain is positive the value of H amounts to 1, otherwise the value is 0. With this extension it is ensured that the creep damage only increases when the component is loaded by tension. The Lemaitre model is able to describe the interaction between creep and fatigue, because the time dependent creep damage and the cyclic fatigue damage are added after each cycle to form the total damage D. It should be mentioned that the evolution of creep and fatigue damage depends on total damage, which represent a nonlinear creep-fatigue interaction. Additionally the influence of multiaxial stress states is considered by the variable R_V. Table 2 shows the approaches with their formulations and the characteristic input values which are necessary for the determination of the damage.

Table 2: Approaches for the damage evaluation

Approach **Damage**	Formulation of damage	Input data
DIN, ASME, RCC-MR, R5, **fatigue damage**	$D_f = \frac{n}{N_i}$	equivalent strain range $\Delta\varepsilon_v$
DIN, ASME, RCC-MR **creep damage**	$D_{c,TF} = \int_0^{t_{dwell}} \frac{1}{t_r(\sigma,T)} dt * n$	stress σ, temperature T, rupture time tr, holding time t_{dwell}
R5, strain based ductility exhaustion approach **creep damage**	$D_{c,DE} = \int_0^{t_{dwell}} \frac{\dot{\varepsilon}_c}{\varepsilon_r(\dot{\varepsilon}_{in},T)} dt * n$	strain rate $\dot{\varepsilon}$, Bruchdehnung ε_r
Lemaitre, **fatigue damage**	$dD_f = \frac{R_V}{\Omega(1-D)^{\alpha_1}} \frac{\left(\frac{\Delta p}{2}\right)^{\gamma+1}}{\gamma+1} dN$	plastic strain range Δp
Lemaitre, **creep damage**	$\dot{D}_c = \frac{R_V}{(1-D)^{\alpha_2}} \left(\frac{\sigma_{eq}}{\lambda}\right)^r H(\varepsilon_1)$	equivalent stress von Mises, Heaviside function H
Lemaitre, consideration of **multiaxiality**	$R_V = \frac{2}{3}(1+\nu) + 3(1-2\nu)\left(\frac{\sigma_H}{\sigma_{v,M}}\right)^2$	material dependent parameter Ω, α_1, γ, α_2, λ, r

The results of the damage evaluation at the two selected positions at the bore holes in the parts made of Alloy 617 B and Alloy C263 and the lifetime analysis are summarized in Table 3. In addition to the tolerable number of cycles up to crack initiation, the creep and fatigue damage are shown.

The results show at the edge of the bore holes in the area of Alloy 617 B that ASME and RCC-MR approaches, which use material-dependent limit curves, calculate higher creep damage compared to fatigue damage portion. The approach according to the R5 method and the Lemaitre model, which have been determined on the basis of independent material limit curves show that the fatigue damage portion is dominant.

If the determined lifetimes are compared, it could be seen that the hole edge in the area of the Alloy C263 has a greater number of cycles to crack initiation compared to Alloy 617 B. Regarding the damage, the fatigue damage portion is greater as the creep damage portion for Alloy C263. The evaluation by means of the approach R5 and the Lemaitre model even showed that the creep damage in fact has no effect on the total damage.

According to the ASME approach the damage is almost evenly distributed, but the creep portion is slightly larger. The comparison of the lifetimes obtained through the various inelastic approaches shows that the

ASME approach leads to the smallest lifetimes in both material areas and the approach of the R5 to the greatest lifetimes. The lifetimes calculated with the approach of the Lemaitre model and the RCC-MR are between the results of ASME and R5, the Lemaitre model provides greater lifetimes.
From the comparison of lifetimes determined for both materials by the the elastic approach of DIN EN 12952 the tolerable number of cycles up to crack initiation is the lowest at the hole edge of Alloy 617 B. The tolerable numbers of cycles in case of this elastic approach are significantly larger than the number of cycles of inelastic approaches at all hole edges. Furthermore, it should be noted that according to the DIN EN 12952 at the hole edge of Alloy 617 B the fatigue damage is dominant and at the hole edge of Alloy C263 the creep damage is dominant. For the hole edge of Alloy 617 B, the damage distribution coincides with the results of inelastic approaches, whereas a completely contrary distribution was determined at the hole edges from Alloy C263.

Table 3: Summary of the calculated lifetimes

	Approach	**ASME**	**RCC-MR**	**R5**	**Lemaitre**	**DIN EN**
	simulation	**inelastic**				**elastic**
Position	**damage envelope -**	**material dependent**		**material independent**		
Alloy 617 B row 3, radius 3 mm (Fig. 8)						
Cycles to crack initiation	**N_a / -**	128	204	769	456	1885
Fatigue damage	**D_f / -**	0,06	0,09	0,70	0,94	0,95
Creep damage	**D_c / -**	0,47	0,16	0,30	0,06	0,05
Alloy C263 row 4 , radius 3 mm (Fig. 8)						
Cycles to crack initiation	**N_a / -**	106	536	1703	770	5336
Fatigue damage	**D_f / -**	0,10	0,50	1,00	0,98	0,41
Creep damage	**D_c / -**	0,11	0,06	0,00	0,02	0,59

One of the difficulties in comparing the methods used for the evaluation and source of differences is the crack initiation criterion. This is not unique for all methods. The application of the material-dependent and -independent properties as well as the type of analysis to be performed (elastic, inelastic) is different.

Comparison numerical and metallographic results

The contour plots of principal stresses obtained from the inelastic analysis (see Section 3.3) show that the highest stresses occur on the hole edges in the two material regions (Fig. 10 a and Fig. 11 a). It should be noted that the stresses in the area of Alloy C263 are larger at the maximum as those of Alloy 617 B. The size and extension of the cracks in both materials is in good agreement with the numerical damage assessment or the distribution of stresses, respectively. Thus, the first principal stress correlates very well with the damage observations. The comparison of the damage evolution from the numerical investigations with the metallographic findings showed that in case of both materials the approaches R5 and Lemaitre delivered correct predictions, small proportions of creep damage in total damage are observed.

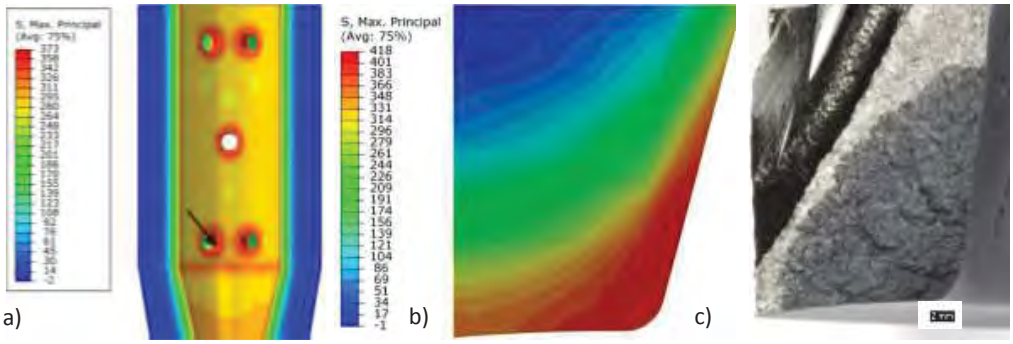

Figure 10: a) contour plots of the maximum principal stress in the inner region of the header Alloy 617B; b) stress distribution at the hole edge, row 3, left r = 3mm, see Fig. 8; c) macroscopic image of the crack surface

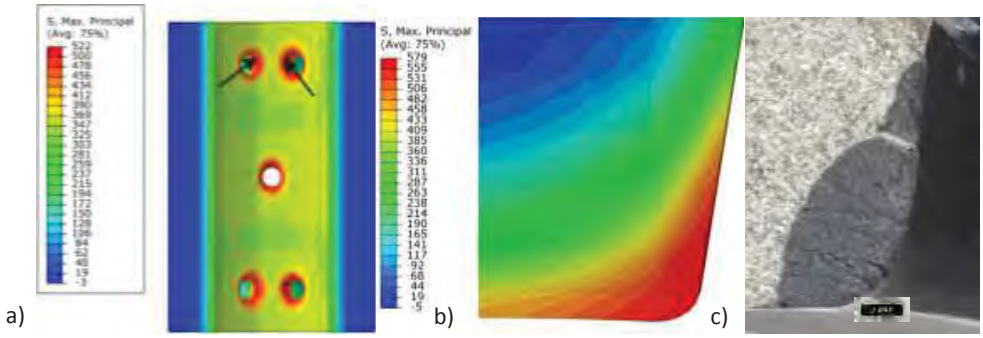

Figure 11: a) contour plots of the maximum principal stress in the inner region of the header Alloy C263; b) stress distribution at the hole edge, row 3, left r = 3mm, see Fig. 8; c) macroscopic image of the crack surface

SUMMARY AND CONCLUSIONS

In the test loop HWT II, which was installed in GKM power plant in Mannheim, thick-walled components made of nickel alloys were operated at temperatures up to 725 °C. The operation mode chosen (creep-fatigue) was to simulate a large number of start-ups and shutdowns with high gradients as expected for future high efficient and flexible power plants. The damage evolution in a header which was made of two nickel alloys 617 B and Alloy C263 was determined and estimated using different analytical and numerical assessment methods. The component was a part of the test loop and was investigated by means of destructive and nondestructive techniques. It was found that fatigue damage is dominant and creep damage only occurs depending on the local stress situation.

Moreover, in this work, the damage was assessed by using numerical methods. Different evaluation approaches for lifetime assessment under creep-fatigue loading were used and compared. It could be shown that the results of the approaches from the standards and codes are not in all cases appropriate in its current form for nickel-based alloys due to conservative or nonconservative predictions. For this reason, the rules for the new materials should be revised.

Using a material model the areas of maximum stresses were identified and an estimated number of cycles up to crack initiation could be reliably predicted for the component. These results are thereby in good correlation with findings determined by nondestructive testing and metallographic investigations.

REFERENCES

[1] VdTÜV Werkstoffdatenblatt Nr. 573, Hochwarmfeste Nickelbasislegierung NiCr23Co12Mo; Werkstoff-Nr. 2.4673, 09.2013.

[2] DIN EN 10302, Warmfeste Stähle, Nickel- und Cobaltlegierungen, 2008.

[3] Chaboche, J. L., "Viscoplastic Equations for the Description of Cyclic and Isotropic Behavior of Metals", Bulletin de l'Académie Polonaise des Science, Série des Science techniques, Vol. XXV, No.1 (1977).

[4] Nouailhas, D., "Unified Modelling of Cyclic Viscoplasticity, Application to Austenitic Stainless Steels", Int. J. of Plasticity, Vol. 5 (1989), pp.501-520.

[5] Ohno, N., "Constitutive Modelling of Cyclic Plasticity with Emphasis on Ratchetting", Int. J. Sci. Vol. 40. (1998), pp. 251-261.

[6] VDI-Wärmeatlas, Verein Deutscher Ingenieure, VDI-Gesellschaft Verfahrenstechnik und Chemieingenieurwesen (GVC), Springer-Verlag Berlin Heidelberg (2006).

[7] DIN EN12952-3, Wasserrohrkessel und Anlagenkomponenten - Teil 3: Konstruktion und Berechnung für drucktragende Kesselteile, Beuth Verlag (2012).

[8] DIN EN12952-4, Wasserrohrkessel und Anlagenkomponenten - Teil 4: Betriebsbegleitende Berechnung der Lebensdauererwartung, Beuth Verlag (2011).

[9] ASME: Part III: Rules for Construction of nuclear facility components, Division 1 – Subsection NH T-1400, American Society of Mechanical Engineers, ASME Boiler & Pressure Vessel Code, ASME International (2011).

[10] RCC-MR, Design and Construction Rules for Mechanical Components of FBR Nuclear Islands. Addendum No. 1, AFCEN (1987).

[11] EDF: Assessment procedure for the high temperature response of structures. UK: Energy Nuclear Generation Ltd., R5, Issue 3 (2003).

[12] Lee, H.-Y.; Y.-W. Kim, K.-N. Song, "Preliminary application of the draft code case for alloy 617 for a high temperature component", Journal of Mechanical Science and Technology 22 (2008), pp. 856-863.

[13] JianPing, J.; Meng Guang, Sun Yi, Xia SongBo, "An effective continuum damage mechanics model for creep–fatigue life assessment of a steam turbine rotor", Int. Journal of Pressure Vessels and Piping 80 (2003), pp. 389–396.

[14] Hüggenberg, D., Ph.D thesis University of Stuttgart, 2016